Molecular Therapy
Nucleic Acids
Original Article

miRNA675-5p inhibitor's dual role as novel therapeutic alternative or sensitizing treatment in resistant glioma models

Cristina Martelli,[1] Marcella Bonanomi,[2] Chiara Pellizzer,[2] Alessandro Giammona,[2,3] Sofia Remedia,[2] Martina Nespoli,[2] Daniela Gaglio,[2] Daniele Capitanio,[4] Danilo Porro,[2,3,5] Luisa Ottobrini,[1,2,6] and Alessia Lo Dico[2,3,6]

[1]Department of Pathophysiology and Transplantation, University of Milan, 20054 Segrate (Milan), Italy; [2]Institute of Bioimaging and Complex Biological Systems (IBSBC)-CNR, 20054 Segrate (Milan), Italy; [3]NBFC, National Biodiversity Future Center, 90133 Palermo, Italy; [4]Department of Biomedical Sciences for Health, University of Milan, 20054 Segrate, Italy; [5]Department of Biotechnology and Biosciences, University of Milano-Bicocca, 20126 Milano, Italy

Glioma is currently the most aggressive CNS tumor. MicroRNA (miRNA)675-5p is a hypoxic miRNA involved in promoting and maintaining the hypoxia inducible factor (HIF)-1α pathway, the driving force for glioma proliferation, migration into surrounding tissue, and resistance. Its inhibition is effective in reducing HIF-1α and all pathways related to it. However, the molecular mechanism through which miRNA inhibition is effective has not yet been fully elucidated. The therapeutic efficacy of the miRNA675-5p inhibitor was tested in a panel of resistant glioma lines evaluating the cellular, molecular, and biochemical rearrangement of the cells after treatment, with particular attention to the oxidative stress imbalance. miRNA675-5p inhibitor has a therapeutic efficacy on its own in resistant cell lines, reducing HIF-1α and its related pathways. The mechanism through which this occurs is the induction of oxidative stress. Its impairment, in fact, reverses the cytotoxic effect. Inhibitor-treated cells acquire metabolic characteristics clearly distinct from untreated cells, triggering compensatory mechanisms that must be considered for the secondary treatment of glioma with temozolomide. The induction of oxidative stress and metabolic rearrangement play key roles in the cytotoxic effect of the miRNA675-5p inhibitor, which could be proposed as a new therapeutic approach in glioma.

INTRODUCTION

Glioma is the most common type of cancer of the CNS. The early stages, grades I–II, are typically self-limiting and can be removed through resection. However, grades III and IV are characterized by a diffuse widespread invasion into the neighboring brain. Therefore, the main problem of the IV degree, known as glioblastoma multiforme (GBM), is the invasion of the surrounding tissue, which is fueled by a high proportion of stem cells and by a strong angiogenic and migratory potential, due to a hypoxic environment. All these features fall back in the establishment of a resistance behavior to standard treatments, with 90% of patients suffering from early disease recurrence.[1–3]

Temozolomide (TMZ) is the most used anti-tumor agent in the treatment of GBM and it is typically associated with radiotherapy. It is part of the STUPP protocol, considered the gold standard in clinical practice. TMZ, is a second-generation imidazotetrazine lipophilic prodrug that acts as an alkylating agent causing lethal DNA damage. As of now, O6-methylguanine-DNA methyltransferase (MGMT) is the most well-established factor that causes TMZ resistance in GBM, since it reverses the methylation-dependent cytotoxicity guided by TMZ.[4] One of the downstream effectors of TMZ is the generation of reactive oxygen species (ROS) that, generally, could have a double effect: on one hand, they can determine tumor progression; on the other hand, in the case of TMZ, they increase the cytotoxic effect of the drug itself.[5,6] In the first case, ROS such as superoxide, hydrogen peroxide, and hydroxyl radical are involved in the switching on of tyrosine kinases such as endothelial growth factor receptor and vascular endothelial growth factor receptor pathways, sustaining GBM progression.[7] On the contrary, as anti-tumoral agents, ROS are involved in further DNA damage and in the enhancement of the cytotoxic effects of TMZ.[8]

There is a strong connection between hypoxia and the pivotal regulator of cell response to hypoxia, hypoxia inducible factor (HIF)-1α, and oxidative stress. Hypoxia is a common feature of the tumor microenvironment in almost all solid tumors, often leading to treatment failure. Due to HIF-1α's ability to modulate different molecular pathways, it plays a role in supporting tumor growth and contributing to the onset of relapses.[9,10]

Several studies showed that hypoxia induces overexpression or down-regulation of various microRNAs (miRNAs), known as

Received 20 November 2024; accepted 25 July 2025;
https://doi.org/10.1016/j.omtn.2025.102647.

[6]Senior author

Correspondence: Alessia Lo Dico, Institute of Bioimaging and Complex Biological Systems (IBSBC)-CNR, 20054 Segrate (MI), Italy.
E-mail: alessia.lodico@cnr.it

hypoxamiRs.[9,11,12] These play a significant role as emerging mediators in the response of tumor cells to the hypoxic microenvironment in various human cancers. HypoxamiRs regulate the expression of genes downstream of HIF-1α, affecting glioma biology. Therefore, targeting the interplay between HIF-1α and miRNAs holds therapeutic potential in glioma treatment. Strategies aimed at inhibiting HIF-1α activity or modulating the expression of specific miRNAs could disrupt tumor-promoting pathways and enhance the efficacy of glioma therapies. miRNA675-5p was identified as a crucial hypoxic miRNA, capable of replicating all physiological changes resulting from decreased oxygen pressure.[13] Inhibition of this miRNA can reduce HIF-1α and its associated pathways. Ultimately, the use of the inhibitor was effective in reducing tumor growth *in vitro* and *in vivo* in a TMZ-sensitive glioma model.[14] However, to date, there is no experimental evidence that the inhibitor can be effective in the treatment of TMZ-resistant gliomas.

To answer this latter question, this paper tested the efficacy of the miRNA675-5p inhibition in a panel of GBM TMZ-resistant cells, suggesting also a possible molecular and biochemical mechanism driving the changes observed at the cellular and molecular levels. Furthermore, regarding the cells that survive after treatment, we speculated about a metabolic rearrangement that could be useful to manage the residual cells responsible for the relapse that often occurs in glioma and makes the treatment of GBM still a challenge in the clinic.

RESULTS

The depletion of HIF-1α induced by the miRNA675-5p inhibitor affects cell viability and aggressive behavior

The experimental setting was designed to include one TMZ-responsive (U251) and three TMZ-resistant (T98, LN18, and U118) cell lines. Intending to screen miRNA675-5p inhibitor efficacy in this panel of glioma lines, first cell viability was assessed. U251 cells have been already investigated observing a decrease in cell viability with a concurrent switch-on of apoptosis-related genes after miRNA675-5p inhibitor incubation.[14]

Similar to what was observed in the TMZ-responsive cells,[14] all the TMZ-resistant cell lines responded to the miRNA675-5p inhibitor treatment with a significant reduction both of cell number (Figure 1A) and cell proliferation, proportional to ATP levels (Figure 1B). Furthermore, an increase in the pro-apoptotic genes *BAX* and *BAD*, as well as the down-regulation of the anti-apoptotic gene *BCL-2* (Figure 1C), has been observed (Figure 1C), as also supported by the induction of caspase-3/7 activity (Figure 1D).

Previous experiments have already highlighted the miRNA675-5p key role in HIF-1α modulation, showing that miRNA675-5p should induce *per se* the cellular, molecular, and biochemical events related to hypoxia.[15]

A study of the interactome (Figure 1E) also supported this hypothesis, highlighting the idea of a relationship between miRNA675-5p and HIF-1α. In particular, we hypothesized that many of the miRNA inhibitor effects could be due to HIF-1α ineffectiveness. Therefore, the transcriptional expression of *HIF-1α* was analyzed by real-time PCR. Molecular data sustained the significant reduction of *HIF-1α* transcript after the miRNA675-5p treatment in U251[13] and in T98, LN18, and U118 cells (Figure 1F). Moreover, its nuclear localization was diminished by treatment with concurrent confinement of this transcription factor in the cytoplasm, in accord with its inactive form (Figure 1G).

In addition, the TMZ-resistant cells treated with miRNA675-5p inhibitor showed a negative modulation of HIF-1α upstream and downstream elements. In particular, we evaluated the mitogen-activated protein kinase (MAPK) signaling cascade genes (Figure 2A), and transforming growth factor β (TGF-β) (Figure 2B): Both pathways decreased after treatment with miR675-5p inhibitor, according to a negative modulation of transactivation and reduced stabilization of HIF-1α, respectively, also at the transcriptional level (Figure 2C). Furthermore, considering that TGF-β regulates epithelial-to-mesenchymal transition (EMT), through MAPK signaling, we analyzed this process by measuring the amount of tubulin in the cell cytoskeleton. The immunofluorescence assay showed an alteration of the normal cell architecture (Figure 2D), confirming the impact of the impairment of HIF-1α, MAPK, and TGF-β.

Another finding about the influence of miRNA675-5p inhibition on the EMT process comes from wounding assays and gene transcription. In detail, all glioma cell lines showed a statistically significant reduction of the migratory ability, analyzed by the wounding assay (Figures 2E and 2F). Molecular analyses showed a contemporaneous decrease in the expression of the *SNAIL*, *SLUG*, and *ZEB1* genes, with an increase in the *E-CAD* gene, after miRNA675-5p inhibition in all the cell lines (Figure 2G). Altogether, these data indicate a less aggressive mesenchymal phenotype mediated by miRNA675-5p inhibitor treatment.

miRNA675-5p inhibition drives its anti-tumoral effect by the induction of ROS levels

Among the processes able to stabilize HIF-1α,[16] we investigated the release of ROS. We observed an increase of ROS levels in both the sensitive and resistant cells after treatment with the miRNA675-5p inhibitor (Figure 3A). In accordance, molecular assays showed down-regulation of some of the genes involved in ROS detoxification, such as *Superoxide Dismutase 1* (*SOD-1*) and *Catalase* (*CAT-1*) (Figure 3B). In addition, real-time PCR analysis supported what we previously observed, reporting the significant down-regulation of some anti-oxidant factors such as the *nuclear factor kappa-light-chain-enhancer of activated B cells (NF-kB*) and *Nuclear factor erythroid 2-related factor 2* (*NRF2*, *NFE2L2*) (with a concomitant, significant increase in *KEAP-1* transcriptional expression, which allows the selective inhibition of NRF2 activity) (Figure 3C).

Therefore, we investigated whether the effect of the inhibitor was principally mediated by the triggering of the oxidative stress switch on. For this reason, we tried to block the miRNA675-5p inhibitor ROS release by the mitochondrion by concomitantly treating cells

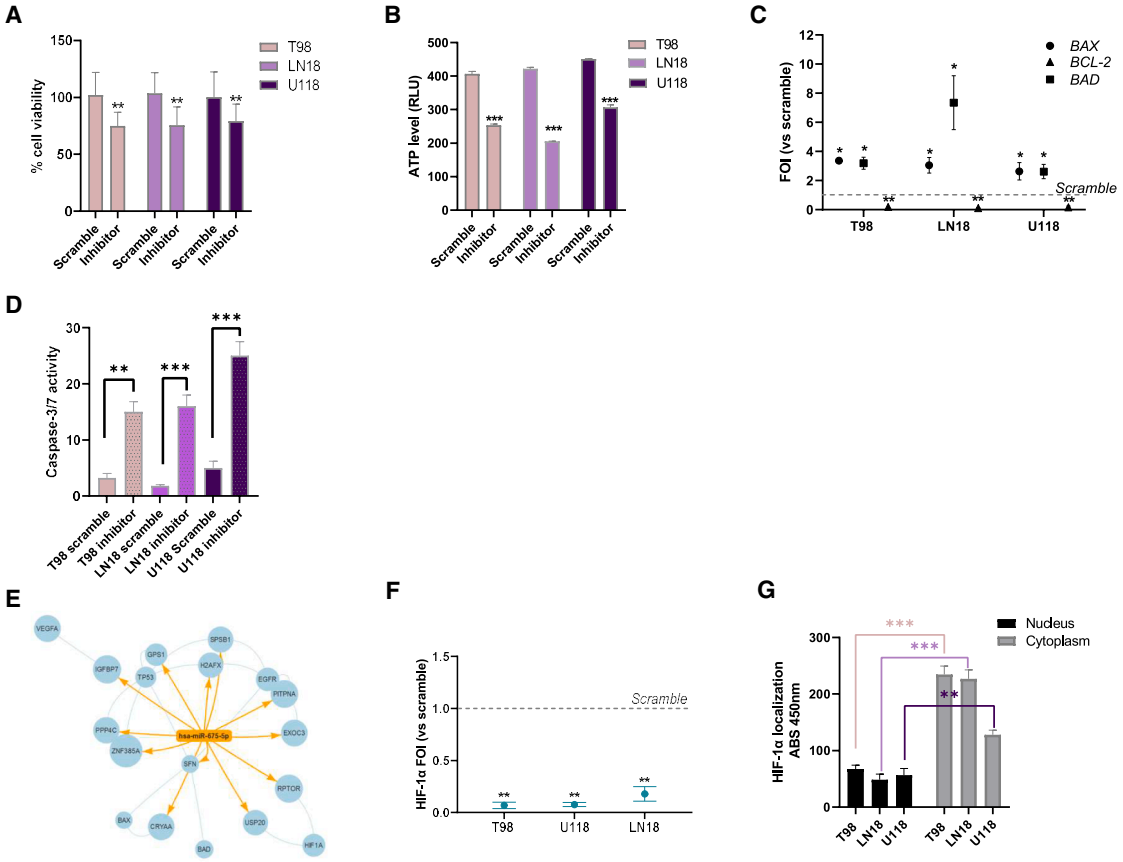

Figure 1. miRNA657-5p inhibitor has an anti-proliferative effect mediated by HIF-1α down-regulation

(A) Viability of TMZ-resistant glioma cell lines (T98, LN18, and U118) cells, assessed by means of Trypan blue exclusion test, and expressed as the percentage of viable cells compared with untreated cells after treatment with miRNA675-5p inhibitor for 18 h. $^{**}p < 0.01$ vs. scramble-treated cells. (B) ATP level in T98, LN18, and U118 cells analyzed by Cell Tox Green kit and expressed as relative fluorescence units compared with scramble-treated cells. $^{***}p < 0.001$ vs. control cells. (C) Gene expression analysis for *BAX*, *BAD*, and *BCL-2* analyzed by real-time PCR in T98, LN18, and U118 cells after treatment with miRNA675-5p inhibitor. Data were normalized to *β-ACTIN*, and the ΔΔCt values were expressed as fold of induction (FOI) of the ratio between treated and scramble-treated cells. $^{*}p < 0.05$; $^{**}p < 0.01$ inhibitor- vs. scramble-treated cells. (D) Analysis of caspase 3/7 activity evaluated by Caspase-Glo 3/7 Assay and expressed as relative luminescent units. $^{**}p < 0.01$ and $^{***}p < 0.001$ inhibitor- vs. scramble-treated cells. (E) *In silico* analysis of an integrative map reconstructed after the public database (The Cancer Genome Atlas Program) interrogation based on protein-protein interaction (called interactome). (F) Gene expression analysis for *HIF-1α* analyzed with real-time PCR in T98, LN18, and U118 cells after treatment with miRNA675-5p inhibitor. Data were normalized to *β-ACTIN*, and the ΔΔCt values were expressed as the FOI of the ratio between treated and scramble-treated cells. $^{**}p < 0.01$ inhibitor- vs. scramble-treated cells. (G) ELISA-based HIF-1α nuclear (black columns) and cytoplasm (gray columns) quantification after miRNA675-5p inhibitor treatment. The data are expressed as absorbance at 450 nm. $^{**}p < 0.01$ and $^{***}p < 0.001$ vs. control cells in nuclear vs. cytoplasmatic localization.
Graphs represent mean values ± SD of three independent experiments.

with the mitochondrial scavenger MitoTEMPO.[17] Unsurprisingly, we observed a statistically significant restoration of ATP release (Figure 3D) when the cells were treated with miRNA675-5p inhibitor and MitoTEMPO. The increase of mitochondrial ROS is also related to the induction of pro-apoptotic genes. Indeed, real-time PCR assays for apoptotic genes confirmed these data, showing a decrease in the pro-apoptotic gene *BAX* and *BAD* and an increase in the *BCL-2* anti-apoptotic factor, in all the glioma cells treated with miRNA675-5p inhibitor in the presence of MitoTEMPO (Figure 3E).

To validate these findings, we analyzed the level of the anti-oxidant molecule glutathione (GSH) by a biochemical approach. This assay reported a statistically significant GSH increase after miRNA675-5p inhibition in all the treated cells (Figure 3F). The observed increase is higher in resistant T98 cells that already have higher ROS levels. It is worth noting that, along with the increase of the reduced form of GSH, we observe also higher levels of its oxidized form (GSSG). The GSH/GSSG ratio, a well-established marker of oxidative stress, increases in U251 cells after treatment with the inhibitor, and remains unchanged after the same treatment in the T98 cell line compared with the control (Figures 3G and 3H). This further supporting the hypothesis that miRNA675-5p inhibitor can alter anti-oxidant defenses.

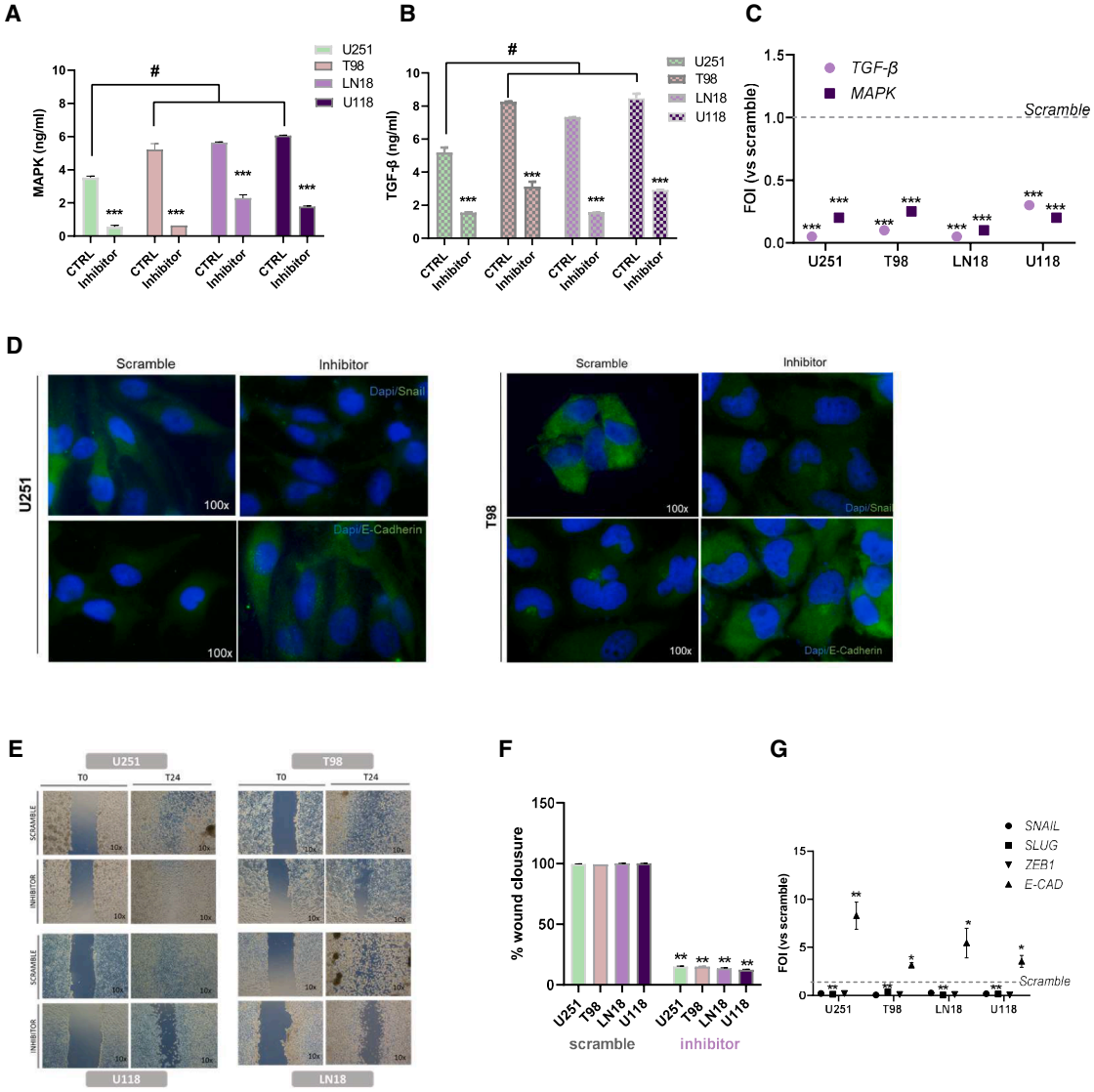

Figure 2. miRNA675-5p inhibitor is efficacy effective in controlling on cell motility

(A) ELISA for human MAPK and (B) for human TGF-β. The concentration of the target substance (expressed as ng/mL), in scramble (CTRL) or miRNA675-5p inhibitor-treated cells, is proportional to the OD450 value. ***$p < 0.001$ vs. scramble treated cells (CTRL); #$p < 0.05$ of U251 CTRL vs. resistant cell line CTRL. (C) Gene expression analysis for *TGF-β* and *MAPK* analyzed by real-time PCR in all cells. Data were normalized to *β-ACTIN*, and the ΔΔCt values were expressed as fold of induction (FOI) of the ratio between treated and scramble-treated cells. ***$p < 0.001$ of miRNA675-5p inhibitor-treated vs. control cells. (D) Images of U251 (left) and T98 (right) were acquired at oil 100× magnification with a Nikon Eclipse 80i fluorescence microscope. The first line represents SNAIL staining (green); the second line shows E-CADERIN staining (green). Nuclei are counterstained in blue with DAPI. Cell morphological analysis was performed by using the ImageJ software (NIH). (E and F) Scratch tests were performed after treatments in all glioma cell lines. The wound closure percentage compared with controls was analyzed and quantified (F) with ImageJ software. **$p < 0.01$ treated vs. scramble-treated cells. (G) Gene expression analysis for EMT-related genes (*SLUG*, *SNAIL*, *ZEB1*, and *E-CAD*) analyzed by real-time PCR in all cells. Data were normalized to *β-ACTIN*, and the ΔΔCt values were expressed as the FOI of the ratio between treated and scramble-treated cells. *$p < 0.05$ and **$p < 0.01$ of miRNA675-5p inhibitor-treated vs. control cells. Graphs represent mean values ± SD of three independent experiments.

Analysis of the metabolic and adaptive rearrangements after miRNA675-5p inhibition

Since the three resistant cell lines, T98, LN18, and U118, had the same behavior after treatment with the inhibitor, we chose T98 as a reference cell line for the TMZ-resistant group, as well as because our group has largely characterized T98 cells in several published papers.[18–21] Thus, we explored what happened in U251 and T98 cells after treatment with miRNA675-5 inhibitor to explore their molecular and metabolic rearrangements. The initial metabolic profiling of these cell lines was evaluated using liquid chromatography-mass

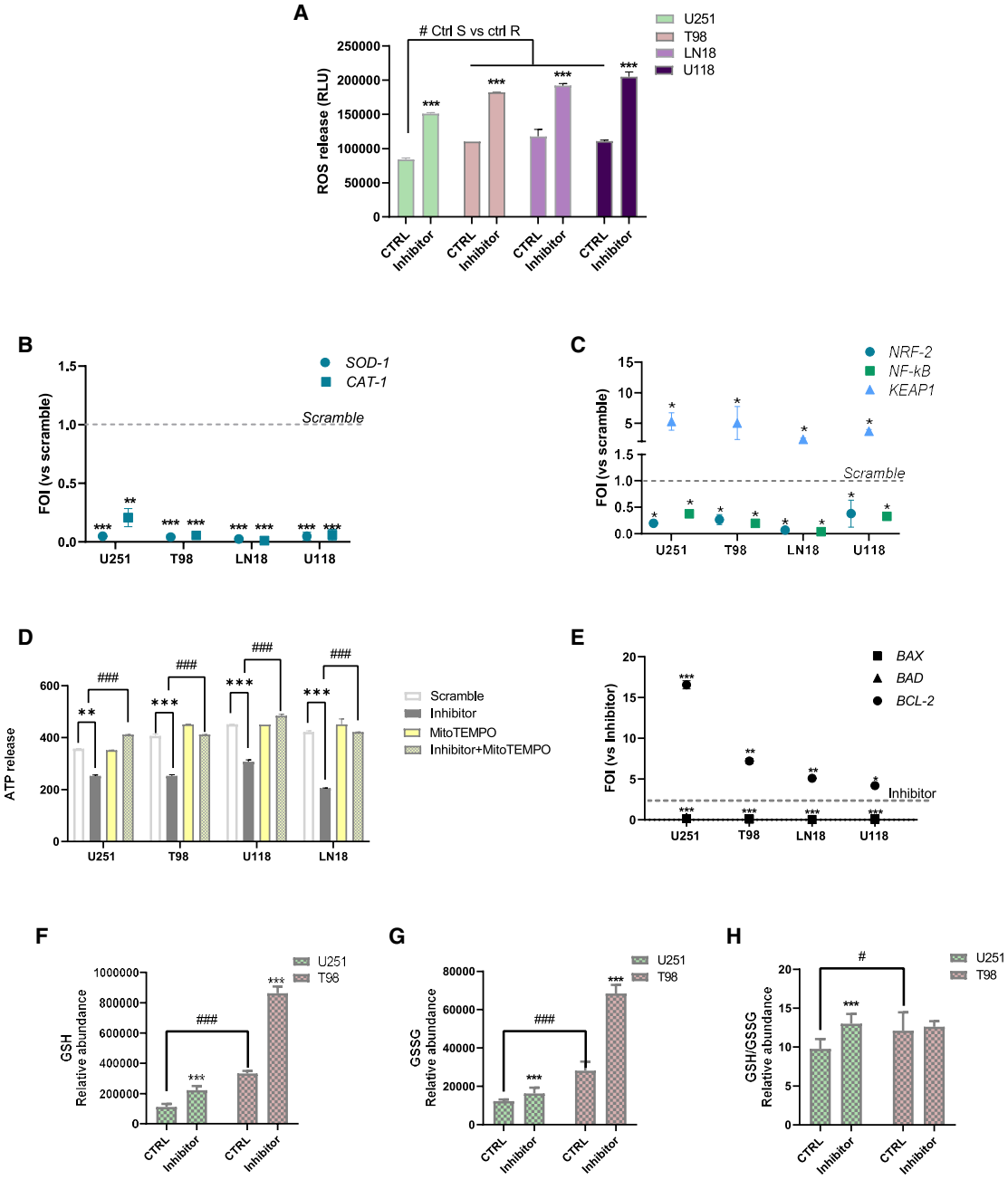

Figure 3. miRNA675-5p inhibitor effect is due to oxidative stress

(A) Luminescent assay (ROS-Glo H2O2 Assay kit) was applied to measure H_2O_2 levels in cell culture medium of different cell lines after treatment with scramble (as control)- or miRNA675-5p inhibitor. Data were expressed as relative luminescence units (RLUs) obtained by luciferase counts normalized for the amount of total proteins quantified by Bradford assay. ***$p < 0.001$ vs. control cells; #$p < 0.05$ U251 vs. average ROS level in T98, LN18, and U118 cells. (B) Gene expression analysis for detox-related genes (*SOD-1* and *CAT-1*) and (C) for HIF-1α-related genes (*NRF-2*, *Nf-kb*, and *KEAP1*) analyzed by means of Real-time PCR in all cells. Data were normalized to *β-ACTIN*, and the ΔΔCt values were expressed as the FOI of the ratio between treated and scramble-treated cells. *$p < 0.05$, **$p < 0.01$; ***$p < 0.001$ vs. scramble-treated cells. (D) ATP levels in U251, T98, LN18, and U118 cells after treatment with MitoTEMPO, a ROS scavenger, and inhibitor analyzed by Cell Tox Green expressed as relative fluorescence units compared with inhibitor-treated cells alone. **$p < 0.01$, ***$p < 0.001$ vs. inhibitor-treated cells; ###$p < 0.001$ inhibitor + MitoTEMPO vs. inhibitor alone. (E) Gene expression analysis of apoptosis-related genes (*BAX*, *BAD*, and *BCL-2*) by real-time PCR in all cells after inhibitor of inhibitor + MitoTEMPO treatment. Data were normalized to *β-ACTIN*,

(legend continued on next page)

spectrometry (LC-MS) metabolomics analysis of control cells. Statistical and enrichment analyses identified 30 metabolites that exhibited statistically significant differences between the two cell lines at the basal level. These metabolites are primarily associated with glutamate metabolism, the Warburg effect, and ammonia recycling (as depicted in Figure S1). Subsequently, we analyzed the metabolic effects of the treatment with miRNA675-5p inhibitor on the two cell lines. In this set of experiments, we introduced the treatment with an miRNA675-5p mimic, aiming to compare the metabolomic changes driven by the presence of up-regulated miRNA675-5p. Hierarchical clustering and principal component analysis for both T98 and U251 cells revealed a more similar metabolic signature between the mimic-treated and scramble cells compared with the miRNA675-5p inhibitor-treated cells (Figure 4A). This observation suggests a significant impact on metabolism in the inhibited cells, whereas the effect of the mimic was minimal. Although the two untreated cell lines display distinct metabolic characteristics (Figure S1), a detailed analysis of the metabolic impact of the inhibitor reveals a reduction in the levels of metabolites associated with the pentose phosphate pathway (PPP) in both cell lines. Specifically, metabolites such as glucose 6-phosphate, ribulose 5-phosphate/xylulose 5-phosphate, and sedoheptulose 7-phosphate exhibit down-regulation (Figure 4B). Along with PPP components, a dramatic reduction of amino acids associated with anti-oxidant machinery (specifically serine, glycine, cysteine, and proline) was observed in inhibitor-treated cells compared with control ones (Figure 4C).

Starting from the assumption that the uncontrolled growth and division of the cells supports their ability to spread and migrate throughout the body, changes in the cell cycle were studied in U251 and T98 cells. Notably, cells responded to miRNA675-5p inhibitor with a reduction of S phase and an increase in the percentage of cells in G0/G1 and G/2 phase, suggesting that the cells are thus less cycling (Figure 4D).

Metabolic rearrangement in the residual cells to maintain redox balance and cell survival after miRNA675-5p inhibitor treatment

miRNA675-5p inhibition influences not only the anti-oxidant machinery but also the level of several metabolites, producing a metabolic rearrangement.

After treatment with the inhibitor, an up-regulation of glutamine metabolism has been observed, with remarkably increased levels of glutamine and glutamate in treated cells compared with the controls, across both cell lines (Figure 5A). Additionally, an increase in the levels of tricarboxylic acid (TCA) cycle intermediates has been measured (Figure 5B). It is also noteworthy that there has been an increase in lactate levels (Figure 5A), which is likely the result of glutaminolysis. The elevation in TCA cycle intermediates and lactate levels is statistically significant in both cell lines but is markedly more pronounced in the TMZ-resistant cell line. These adaptive responses may collectively represent an attempt to survive, characterized by this distinctive metabolic rearrangement.

miRNA675-5p sensitizes resistant cells to subsequent TMZ treatment

To better understand the molecular profile of T98 cells after treatment with the inhibitor and how these changes may increase their susceptibility to TMZ, we further explored one of the pathways identified by interactome analysis (Figure 1D), the one involving HIF-1α and RPTOR.

The contribution of this protein in the U251 and T98 lines was compared after inhibitor and TMZ treatment (Figures 6A and 6B). U251 and T98 cells presented a different basal level of RPTOR protein, with a greater amount in T98 cells compared with U251 cells. In both cell lines, TMZ failed to produce a statistically significant modulation of the RPTOR protein. miRNA675-5p inhibitor did not modify RPTOR level in U251 cells, while it statistically reduced its level in T98 cells. Combined treatment with TMZ and the inhibitor only in U251 cells induced a statistically significant decrease in RPTOR level while it induced no reduction in T98 cells.

Following, we treated TMZ-resistant T98 cells firstly with the inhibitor and then with TMZ after 24 h of maintenance in fresh medium. Cell viability was then tested after 24 h TMZ treatment and, surprisingly, in both cell lines the treatment showed a significant increase in the percentage of dead cells compared with cells not treated with TMZ (Figures 6C and 6D), and this finding is of particular interest and importance in resistant cell lines. To support these data, gene expression analysis for apoptosis highlighted an increase in the pro-apoptotic genes *BAX* and *BAD* and a reduction in the anti-apoptotic gene *BCL-2* (Figure 6E). The data support the idea that the inhibition of miRNA675-5p can sensitize T98 cells to chemotherapy to which they were previously refractory.

Since miRNA-675-5p is considered a hypoxic miRNA, we also proceeded to analyze the levels of this transcription factor. The study of the expression of *HIF-1α* on both U251 and T98 cells revealed that the two lines have a differential expression of *HIF-1α* at the basal level, with a higher level in T98 compared with U251 cells. Treatment with the miRNA675-5p inhibitor in T98 cells brought *HIF-1α* back to a level comparable with that measured in U251 basally, thus making the two lines similar from the point of view of *HIF-1α* expression. In contrast, a single treatment with TMZ in T98 cells increased this level. Significantly, treating T98 cells with the inhibitor and then with TMZ reduced the level of HIF-1α even more than with the inhibitor alone (Figure 6F).

and the ΔΔCt values were expressed as the FOI of the ratio between MitoTEMPO plus inhibitor and inhibitor-treated cells. (F–H) Relative GSH (F) and GSSG (G) abundance and GSH/GSSG ratio (H) in U251 and T98 cell line in control condition vs. inhibitor-treated cells obtained by LC-MS analysis ($n = 9$). ***$p < 0.001$ vs. scramble-treated cells; #$p < 0.05$ and ###$p < 0.001$ U251 scramble-treated (control) cells vs. T98 scramble-treated (control) cells.
Graphs represent mean values ± SD of three independent experiments.

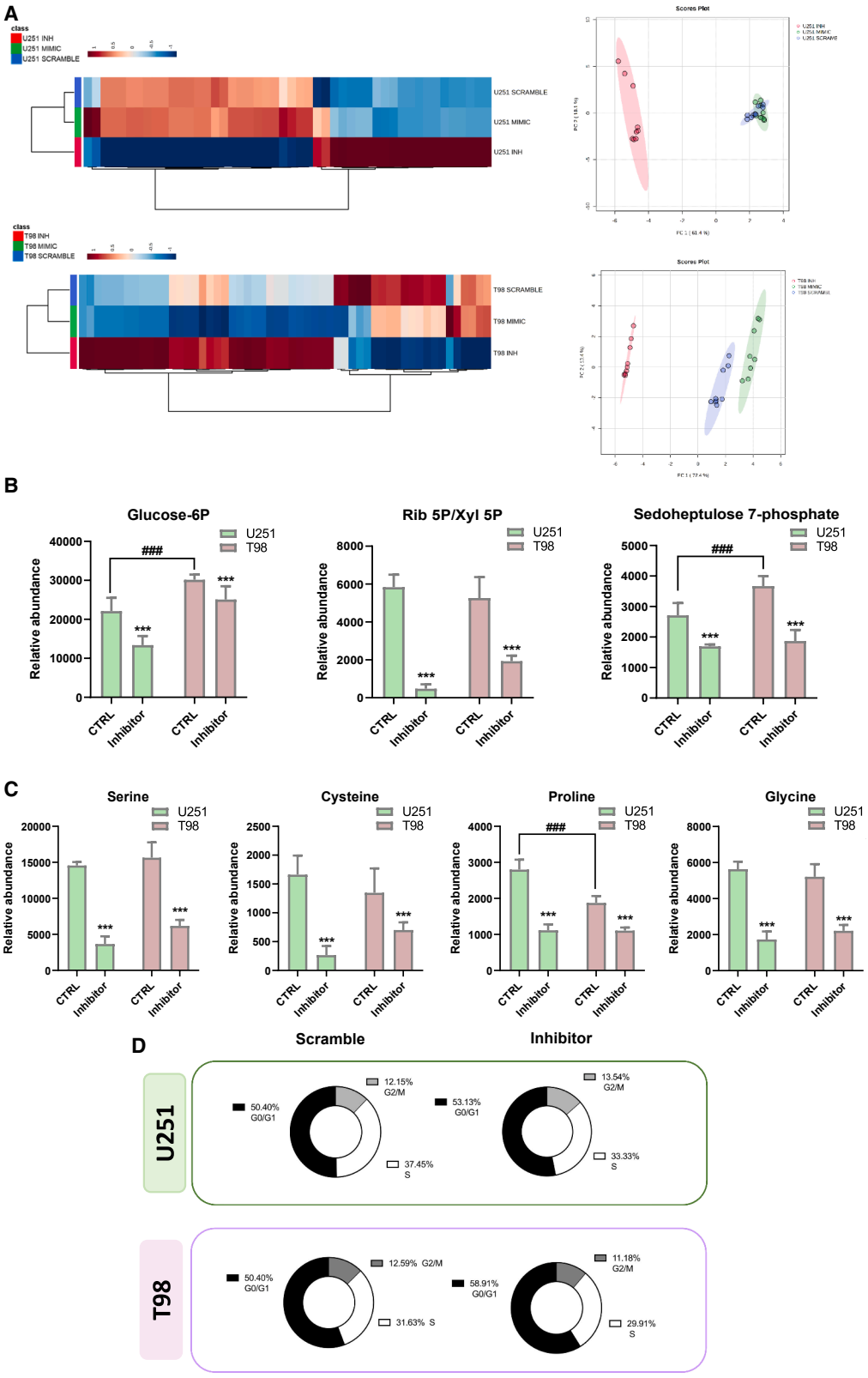

(legend on next page)

By evaluating the expression level of miRNA675-5p and HIF-1α in T98 cells, we observed a statistically significant reduction of both molecules after treatment with TMZ only when it occurred after inhibition treatment and refresh period (Figure 6G). In contrast, T98 cells directly treated with TMZ showed an increase in viability and HIF-1α expression as well as activity after 24 h of treatment with TMZ),[18,19] supporting the idea that prior inhibition of miRNA675-5p sensitized the cells to TMZ.

DISCUSSION

Treatment of glioma remains a challenge in oncology research. The identification of new therapeutic strategies, aimed at overcoming the inevitable establishment of resistance and the onset of relapses, is of extreme importance. In fact, the first-line treatment for a newly diagnosed glioma, irrespective of histological grade, involves TMZ; however, resistance occurs, resulting in tumor growth and progression. In addition, even if a large area beyond the tumor is usually included in a maximally safe surgical resection,[22] the extent of surgery is inevitably limited by the cerebral anatomy,[23] and infiltrated residual cells often give rise to recurrence.[24]

In this context, the work presented herein describes the efficacy of miRNA675-5p inhibition in a panel of GBM cell lines known to be resistant to TMZ, also describing the molecular and metabolic rearrangement after treatment.

The effectiveness of this miRNA inhibitor has been already demonstrated by our group in a TMZ-sensitive model both *in vitro* and *in vivo*.[14] Since the efficacy of this inhibitor was comparable with that of TMZ, we studied its efficacy on resistant cell lines.

Three glioma lines, characterized to be resistant to TMZ and to have similar genetic backgrounds but different percentages of MGMT promoter methylation, were subjected to miRNA675-5p inhibition; afterward cellular, molecular, and biochemical assays were performed. Treatment with miRNA675-5p inhibitor reduced glioma cell viability and cell ATP levels. Remarkably, the inhibition of miRNA675 not only intervenes in a possible slowing of growth but also promotes apoptosis, as supported by the negative modulation of *BCL-2*, similar to that observed in several anti-tumor therapies.[25]

Resistance to therapies often manifests itself not only with a non-reduction of HIF-1α but even with its induction.[18] Herein, we demonstrated that treatment with the miRNA675-5p inhibitor reduced HIF-1α expression and its nuclear translocation, which is necessary for its activity. Contemporaneously, we observed that both MAPK/extra-cellular signal-regulated kinase (ERK) and TGF-β pathways are decreased, highlighting that miRNA675-5p inhibition acts up-stream to HIF-1α. This sheds light on the fact that the inhibitor exerts its activity not in a direct way on the transcription factor but through the inhibition of one of its activation molecules and confirms that its activity plays a part, among other things, in the proliferation processes of gliomas.[26,27] In addition to the influence on proliferation, the MAPK/ERK pathways also regulate the EMT, and we showed that the miRNA675-5p inhibitor is endowed with the ability to modulate the migratory potential of cells as well. Indeed, the inhibitor reduced the mesenchymal-like characteristics associated with cell migration, since expression of pro-mesenchymal genes such as *SNAIL*, *SLUG*, and *ZEB1* were significantly compromised by the treatment. On the contrary, the epithelial phenotype was favored by the increase in the expression and activity of E-cadherin.[28] These modulations reduce cell mobility and migratory ability.

Since tumor cells often exhibit a dysregulated redox balance compared with normal cells, ROS modulation is an intriguing approach for the treatment of glioma. For instance, the combination of ROS-modulating agents with traditional chemotherapy or targeted therapy may overcome resistance mechanisms and improve treatment outcomes.[29,30] In our hands, the resistant cell lines respond to the inhibitor with an increase in the release of ROS and a concomitant slowdown, at the transcriptional level, of the detoxification system mediators. In particular, it should be noted that *NRF2*, the most well-known regulator[31,32] of the oxidative stress-induced system, is negatively modulated by the treatment, as supported by the literature.[33–37] Moreover, recent studies have highlighted the negative prognostic role of NRF2, since its inhibition could be considered as a strategy to induce oxidative stress and processes related to cell death, also in glioma.[38,39]

To study the leading role of oxidative stress within the effect of the miRNA675-5p inhibitor, we treated cells with a mitochondrial ROS scavenger, MitoTEMPO. In TMZ-resistant cells, ROS scavenging with MitoTEMPO nullifies miRNA675-5p inhibitor activity. This result suggests that the presence of ROS in the glioma cells,

Figure 4. Analysis of metabolic and adaptive rearrangements after miRNA675-5p inhibition

(A) (Left) Untargeted metabolic profiling shown as a hierarchical clustering heatmap containing significantly different intracellular metabolites as detected by LC-MS in U251 cells (top) or T98 cells (bottom) treated with scramble vs. inhibitor vs. mimic. Colors represent different levels that increase from blue to red. (Right) Principal component analysis scores plot between the first two principal components in U251 cells (top) or T98 cells (bottom) treated with scramble vs. inhibitor vs. mimic. The explained variances are shown in brackets on title axis. Heatmaps and PCAs were obtained by Metaboanalyst 5.0. (B and C) Relative abundance of metabolites involved in PPP pathway (B) (glucose-6P, ribulose-5P and xylulose-5P ratio, and sedoheptulose-7P) and amino acids involved in redox metabolism (C) (serine, cysteine, proline, and glycine) in U251 and T98 cells treated with scramble- vs. inhibitor-treated cells obtained by LC-MS ($n = 9$). ***$p < 0.001$ vs. scramble-treated cells; ###$p < 0.001$ U251 scramble-treated (control) cells vs. T98 scramble-treated (control) cells. (D) Cell cycle measured with propidium iodide labeling of scramble- or inhibitor-treated cells analyzed by FACSCalibur flow cytometer (BD Biosciences) on U251 (top) and T98 cells (bottom).

Graphs represent mean values ± SD of three independent experiments.

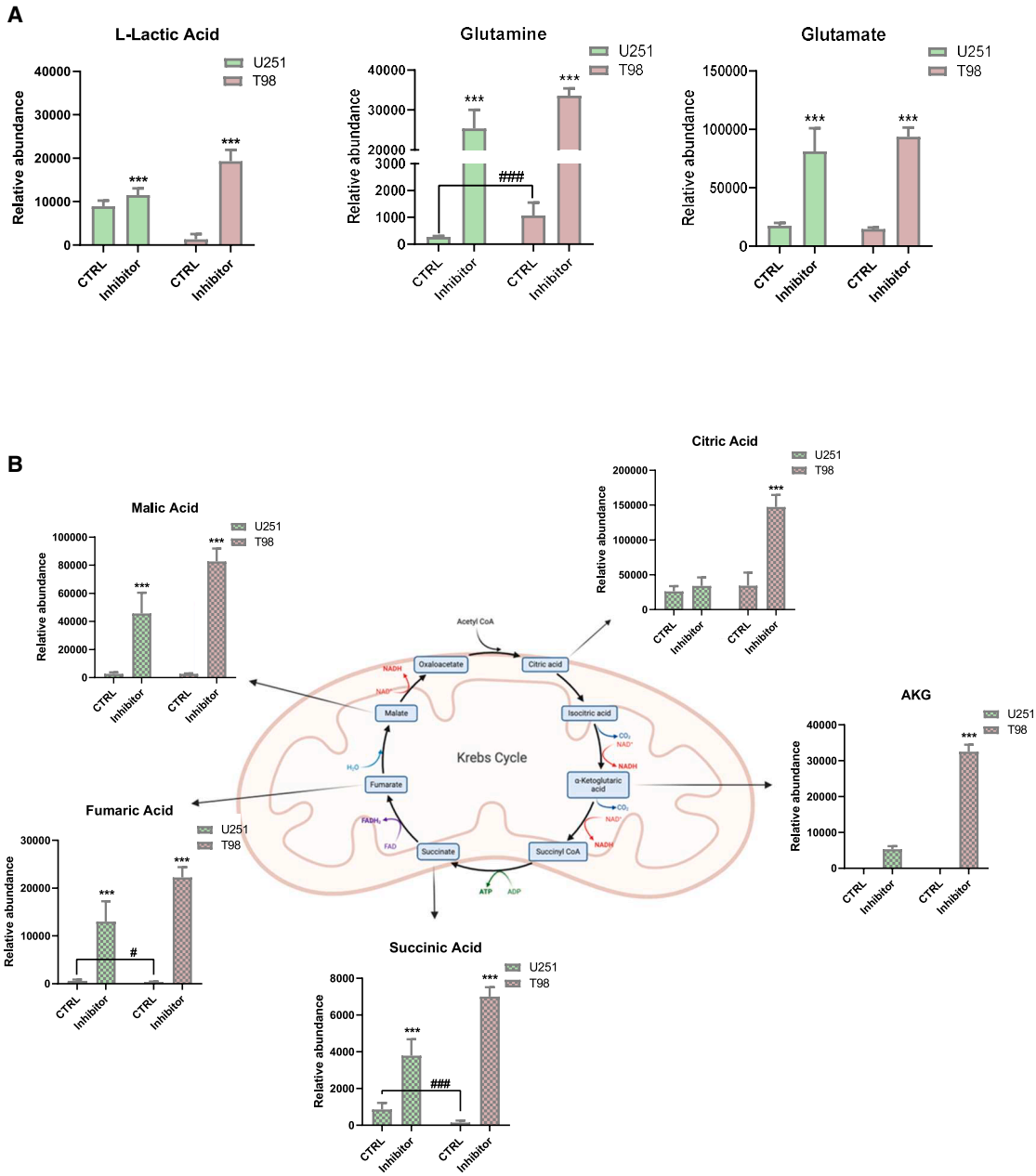

Figure 5. Analysis of amino acid and TCA component levels after miRNA675-5p inhibition

(A) Relative abundance of the amino acids glycine (left), glutamate (center), and glutamine (right), and (B) TCA cycle components (citric acid, α-ketoglutarate [AKG]-succinic acid, fumaric acid, and malic acid) in U251 and T98 cells treated with scramble or inhibitor obtained by LC-MS (n = 9). ***p < 0.001 vs. scramble-treated (CTRL) cells; #p < 0.05 and ###p < 0.001 U251 scramble-treated (control) cells vs. T98 scramble-treated (control) cells.

Graphs represent mean values ± SD of three independent experiments.

probably induced by miRNA675-5p inhibitor, is necessary for its efficacy.

Another issue concerning GBM management is the ability of those cells to adapt to anti-tumor treatments by implementing cellular, molecular, and biochemical rearrangements, as well as the reprogramming of several adaptative processes.[40] This metabolic and molecular plasticity observed in cells that survive after miRNA675-5p inhibition can be studied to comprehend how cells respond to the treatment and to develop efficient strategies to face these cells to limit minimal residual disease or recurrences.

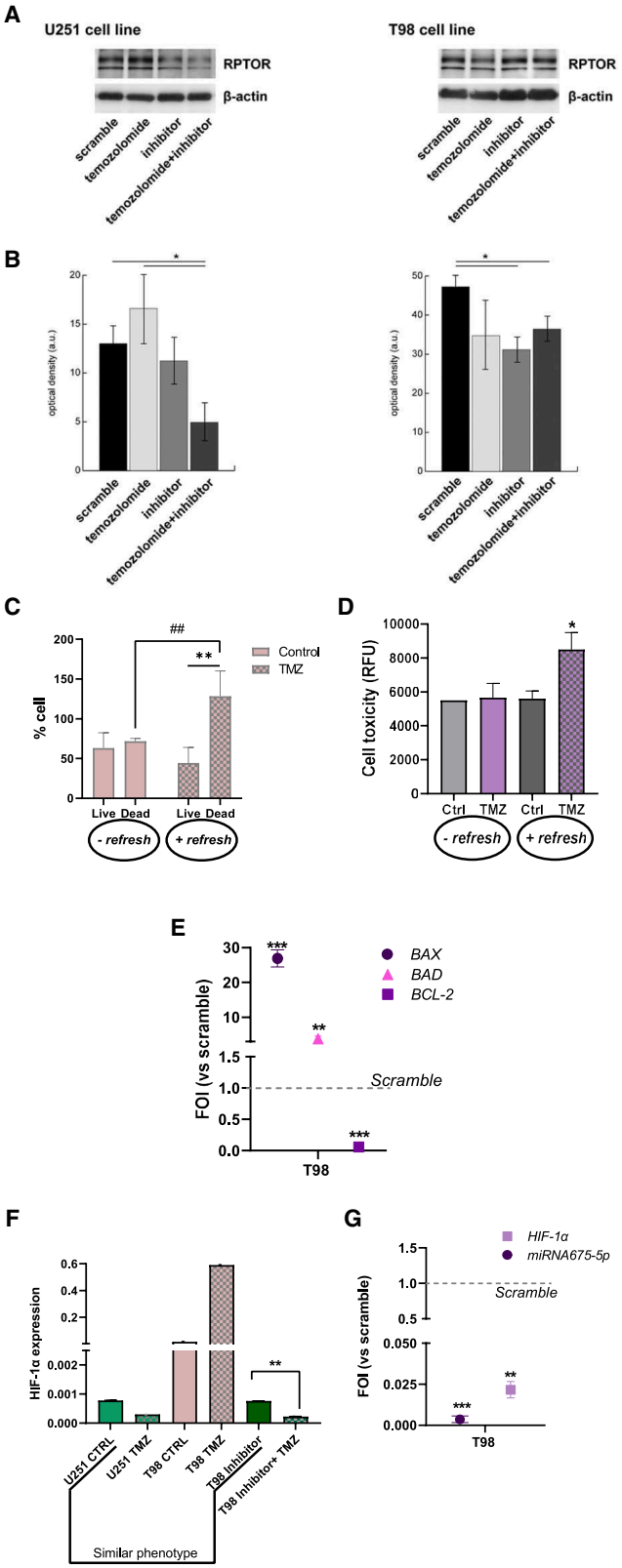

Figure 6. miRNA675-5p sensitizes resistant cells to subsequent TMZ treatment

(A and B) Representative images of immunoblots (A) and quantification histograms (B) of *regulatory associated protein of mtor complex 1* (RPTOR) expression. RPTOR level was assessed in U251 (left) and T98 (right) scramble (black bars) cell lines, treated with TMZ (light gray bars) miRNA675-5p inhibitor (gray bars), or inhibitor followed by TMZ treatment (dark gray bars). Mean ± SD. *Significant difference, ANOVA and Tukey's test, $n = 3$, $p < 0.05$. (C) Viability of resistant glioma cell lines (T98) cells, assessed by means of Trypan blue exclusion test, and expressed as live or dead cells after miRNA675-5p inhibition and subsequent TMZ challenge, in absence or presence of the refresh period. $^{**}p < 0.01$ dead vs. live cells; $\#\#p < 0.01$ dead cells in control vs. TMZ-treated cells. (D) Cytotoxicity evaluation of the average of T98, LN18, and U118 cells analyzed by Cell Tox Green expressed as relative fluorescence units (RFUs) compared with scramble-treated cells, in absence or presence of the refresh period. (E) Gene expression analysis of apoptosis related genes (*BAX*, *BAD*, and *BCL-2*) by real-time PCR in all cells after TMZ treatment subsequent to miRNA675-5p inhibition. Data were normalized to *β-ACTIN*, and the ΔΔCt values were expressed as fold of induction (FOI) of the ratio between inhibitor + TMZ- and scramble + TMZ-treated cells. $^{**}p < 0.01$, $^{***}p < 0.001$ of inhibitor + TMZ- vs. scramble + TMZ-treated cells. (F) Comparison of *HIF-1α* expression level between U251 basal level and T98 basal and treated cells. Data were normalized to *β-ACTIN*, and the ΔCt values were depicted in the graph. $^{**}p < 0.01$ inhibitor alone vs. inhibitor + TMZ treatment. (G) Gene expression analysis of *HIF-1α* and *miRNA675-5p* levels by real-time PCR in all cells after TMZ treatment subsequent to miRNA675-5p inhibition. Data were normalized to *β-ACTIN or U6*, respectively housekeeping reference for gene and miRNA expression, and the ΔΔCt values were expressed as FOI of the ratio between inhibitor + TMZ- and scramble + TMZ-treated cells. $^{*}p < 0.05$, $^{***}p < 0.001$ inhibitor + TMZ-vs. scramble + TMZ-treated cells.

Since we stated that an increase in the ROS level is fundamental in the effect of miRNA675-5p inhibitor, the level of GSH, a leading detoxification factor, was first evaluated. Cells respond to miRNA675-5p inhibitor by trying to increase GSH levels. However, the counterpart GSSG (deriving from oxidation of GSH) was also increased, indicating that the cellular redox status was altered. This supports the efficacy of the miRNA675-5p inhibitor and underscores the importance of maintaining a balance between pro-oxidant and anti-oxidant molecules. To note, the role of miRNA675-5p has also been discussed in other pathologies characterized by an imbalance in the redox potential. In fact, studies related to myopathies due to gene modulations affecting skeletal muscle,[41] myocardial ischemic injury,[42] and diabetic cardiomyopathy[43] highlighted the relationship between miRNA675-5p and oxidative stress.

For what concerns the metabolic changes in residual cells surviving the treatment, it was evident that the miRNA675-5p inhibitor induces significant metabolic alterations compared with those in scramble- and mimic-treated cells. The metabolic profile is similar between cells in which the presence of miRNA was not altered and cells in which miRNA675-5p was up-regulated, supporting the idea that miRNA675-5p acts to sustain cell viability and growth. Conversely, the inhibition of miRNA675-5p generated a metabolic switch in the residual cells.

In inhibitor-treated cells, we observed a decrease in PPP metabolites and in several amino acids related to redox metabolism. The decrease

in the PPP intermediates determines a reduction of nicotinamide adenine dinucleotide phosphate (NADPH) production, leading to a decrease in the reducing potential of the cells. This impairment supports once again that miRNA675-5p inhibition exposes cells to increased oxidative stress. Along with its role in supporting redox homeostasis, PPP is a key pathway in nucleotides, lipids, cholesterol, and amino acids synthesis, promoting rapid cell proliferation in glioblastomas.[44] It has been demonstrated that GBM exhibits elevated levels of PPP precursors, including 6PG, R5P, X5P, and S7P, consequent to hypoxia.[45] Some evidence in the literature shows that the enzymes of this pathway have already been used as pharmacological targets in GBM,[46] and miRNA675-5p inhibition can be included in the framework of these treatments, which are aimed at down-regulating this pathway. Regulation of redox homeostasis and hypoxia-related metabolism is not limited to PPP but involves several other actors, including amino acids. It has been demonstrated that the serine synthesis pathway is up-regulated in several GBM cell lines under hypoxic conditions, leading to increased levels of serine and glycine within the cell.[47] The activation of this pathway has been shown to enhance nucleotide synthesis and NADPH production, thereby boosting the antioxidative capacity of the cell. In addition, it has been demonstrated that both proliferation and survival are impaired by serine pathway inhibition under nutrient and oxygen deprivation.[47] Cysteine is another essential amino acid in redox homeostasis, as it is a key component of the primary anti-oxidant GSH and also acts as a potent anti-oxidant on its own.[48] Cysteine has been demonstrated to be a limiting factor in the proliferation and survival of gliomas *in vivo*. This is due to the fact that gliomas are incapable of synthesizing cysteine within the cell and thus are reliant on acquiring cystine from the microenvironment.[49] Also, proline has a role in maintaining redox balance in cells, being involved through its synthesis/degradation cycle in the net production of NADP/NADPH.[50] All these amino acids result to have lower levels after miRNA675-5p inhibition thereby reinforcing the role of this treatment in increasing oxidative stress.

In addition to this panel of down-regulated metabolic pathways, which lead to a decreased proliferative capacity of the tumor cells, our metabolomics approach also facilitated the identification of other pathways impacted by the treatment. These may instead be linked to resistance strategies that the cells are implementing for survival. In particular, we observed a concomitant increase of TCA intermediates and glutamine/glutamate levels, indicating a metabolism that could be sustained by glutamine instead of glucose.[51–53] The reduction measured in glucose-6-phosphate and PPP could be due to the observed decreased level of *GLUT-3* expression (data not shown).[54] Glucose deprivation has been shown to stimulate compensatory pathways, including glutaminolysis. This pathway is responsible for the generation of cellular energy from the degradation of glutamine. The process thus enables the replenishment of the TCA cycle through anaplerotic reactions to maintain cycle function.[52] This alternative process has been already described in glioma as a final escape attempt.[44,52,55] The identification of activation of these alternative pathways following treatment has the potential to provide insights into the selection of combination therapy that is more effective than current methods. This could involve the use of a second drug that directly or indirectly targets the newly identified pathways. For instance, the inhibition of glutaminase, the enzyme responsible for converting glutamine into glutamate, has been shown to effectively eliminate glioblastoma stem-like cells. These cells play a critical role in therapy resistance and tumor recurrence, making their eradication essential for improving treatment outcomes and preventing relapse.[56] The combined use of miRNA675-5p and glutaminase inhibitors may be a promising approach that merits further investigation in subsequent studies.

Metabolism and the cell cycle are strongly related, and there is a bidirectional relationship between them. Indeed, after treatment with the inhibitor, the percentage of cells in S phase was reduced, with a greater percentage of cells confined in the G0/G1 phase of the cell cycle. Generally, these cells are considered dormant and resist the effects of chemotherapy and radiotherapy, suggesting an escape mechanism of the cells.[57] However, this status could also indicate senescence, an irreversible status in which cells are arrested.[58] This status could be very interesting in the glioma because it could indicate a lower probability of relapse of the disease. In both cases, combination therapies that target both proliferating and surviving tumor cells at different stages of the cell cycle may be more effective in eradicating glioma and preventing recurrence.

All these data provide clues about the establishment of a less aggressive behavior or a more susceptible phenotype to TMZ therapy in residual cells treated with miRNA675-5p inhibitor, as demonstrated by the analysis of RPTOR levels even in U251 cells that are already sensitive to TMZ.

To note, RPTOR is required for the regulation of mTORC1, whose activation (influencing also HIF-1α activity) has been associated with malignancies.[59–61]

These findings revealed compelling evidence even in previously resistant cells. After treatment with the inhibitor, cells become sensitive to TMZ treatment after a refresh period. This is corroborated by a decrease in viability and an increase in cytotoxicity and in the expression of *BCL-2* and a concomitant increase in *BAX* and *BAD* genes. Furthermore, after the refresh period, sensitized T98 cells showed a HIF-1α expression comparable with that observed in sensitive U251 cells. This could be of extreme importance in the management of glioma patients, since cells could be re-sensitized to TMZ, permitting them to be treated again.

These findings therefore suggest a potential mechanism by which resistant cells can rearrange themselves after treatment with the miRNA675-5p inhibitor. However, further studies will be necessary to definitively characterize how the inhibitor works and how cells recover responsiveness to TMZ.

Considering all our results, it has been demonstrated that the pathway related to oxidative stress and HIF-1α is of extreme

importance both in the induction of the primary cytotoxic effect and in targeting the residual cells. Probably after having developed an attack strategy, it will be necessary to re-modulate the therapeutic strategy considering that the cells acquire different characteristics and behaviors. Understanding the metabolic rearrangements driven in glioma is crucial for developing targeted therapies aimed at disrupting the different involved pathways.

By combining these approaches and continuously exploring new therapeutic avenues, it may be possible to overcome resistance and effectively target residual glioma cells, improving patient outcomes and survival rates.

MATERIALS AND METHODS

Cell lines and reagents

U251 (ICLC, Ospedale San Martino, Genova, Italy), T98, LN18 and U118 ATCC (American Type Culture Collection, Manassas, VA, USA) were maintained in RPMI1640 (U251 and T98) or DMEM High Glucose (LN18 and U118), both supplemented with 10% heat-inactivated fetal bovine serum, 100 U/mL penicillin and 100 mg/mL streptomycin, and 2 mM glutamine (all Euroclone, Milan, Italy) in a humidified atmosphere of 5% of CO_2 at 37°C.

Cell transfection

For cell transfection, Attractene Transfection Reagent (cat. number 1051531, Qiagen, Hilden, Germany) was used following the manufacturer's indication. Briefly, for all the experiments glioma cells were seeded at 10,000 cells/cm^2 and transfected with 15 pmol/mL of hsa-mir675-5p inhibitor (custom made by Eurofins Genomics, Vimodrone, Milan, Italy), or scrambled negative control (custom made by Eurofins Genomics). Eighteen hours after transfection, the medium was collected and the cells were processed for the following assays.

Cell viability, ROS, and caspase assays

The cytotoxicity of treatments was tested utilizing Cell ToxGreen Cytotoxicity Assay kit and Cell Titer-Glo Luminescent Cell Viability Assay (all Promega, Madison, WI, USA).

The ROS content after all treatments was tested by using ROS-Glo H_2O_2 Assay kit and the caspase 3 and 7 activity was evaluated by using the Caspase 3/7 Assay kit (both from Promega). All assays were performed by using commercially available kits and were carried out according to the manufacturer's instructions.

RNA extraction and real-time PCR

Total RNA was isolated using TRIzol reagent (Life Technologies, Carlsbad, CA, USA) and it was reverse transcribed to cDNA using a High-Capacity cDNA Reverse Transcription Kit (Applied Biosystems, Waltham, MA, USA) and the Mir-X miRNA First-Strand Synthesis Kit (Takara Bio) for miRNA675-5p) following the manufacturer's instructions. The cDNA was diluted and used for the real-time PCR analysis. The real-time PCRs were performed in triplicate for each data point by using the Sybr Green technique; the oligonucleotides used are shown in Table 1. Target mRNA content changes in relation to the *β-ACTIN* or U6 for miRNA675-5p analysis housekeeping gene were determined using the ΔΔCt method (represented as fold of induction and compared with control levels).[62]

HIF-1α quantification

An ELISA-based kit (TransAM Kit, Vinci-Biochem, Florence, Italy) was used to detect and quantify HIF-1α transcriptional factor activity following the manufacturer's instructions. Briefly, nuclear extracts were firstly prepared using the Nuclear Extract Kit (Vinci-Biochem) and 8 μg of the samples were added to the coated plate and analyzed. Data were expressed as HIF-1α protein content in the total nuclear extract (absorbance).

Wounding assay

For the wound healing assay, at the end of the treatment, a wound was created by manually scraping the confluent glioma monolayer with a p200 pipette tip. Images at time zero (t = 0 h) were acquired to record the initial area of the wounds, and the recovery of the wounded monolayers due to cell migration toward the free area was evaluated at 24 h (t = 24 h). The area of wound was quantified by Java's ImageJ software (http://rsb.info.nih.gov, National Institutes of Health [NIH], Bethesda, MD, USA) and the migration of cells toward the wounds was expressed as percentage of wound closure: % of wound closure = $[(A(t = 0\,h) - A(t = 24\,h))/A(t = 0\,h)] \times 100$, where A(t = 0 h) is the area of wound measured immediately after scratching, and A(t = 24 h) is the area of wound measured 24 h after scratching.

Immunofluorescence

We seeded 10,000 cells/cm^2 GBM cells on adherence round glass slides and cultured in with their own media and transfected with hsa-mir675-5p inhibitor or scrambled negative control. Eighteen hours after transfection, the cells were washed by PBS and fixed for 30 min at 37°C with 4% paraformaldehyde. After that, the round glass slides were further washed with PBS and permeabilized with PBS/FBS 5%/Triton 0.3% solution for 10 min at 4°C. After washing with PBS, the cells were incubated with a blocking buffer composed of BSA 2% in PBS tween 0.1% for 30 min at room temperature. The cells were incubated overnight at 4°C with the following primary antibodies against Tubulin (sc-5286, Santa Cruz Biotechnology, Dallas, TX, USA), or E-CADHERIN (SAB4503751, Sigma-Aldrich, St. Louis, MO, USA). Thereafter, cells were labeled with 488 Alexa Fluor-conjugated secondary antibodies (Invitrogen, Waltham, MA, USA) for 30 min at room temperature in the dark. Nuclei were blue counterstained with DAPI (InVitrogen).

Next, cells were washed with PBS and slides were closed with glass coverslips using a clear mount solution (Invitrogen). Images were acquired at oil 100× magnification with a Nikon Eclipse 80i fluorescence microscope. Cell morphological analysis was performed by using the ImageJ software (http://rsb.info.nih.gov, NIH).

Table 1. Primers details

Gene	Forward 5′-3′	Reverse 5′-3′
β-ACTIN	TCAAGATCATTGCTCCTCCTG	CCAGAGGCGTACAGGGATAG
BAD	CCCAGAGTTTGAGCCGAGTG	CCCATCCCTTCGTCGTCCT
BAX	ATGGACGGGTCCGGGGAG	ATCCAGCCCAACAGCCGC
BCL-2	GATTGTGGCCTTCTTTGAG	CAAACTGAGCAGAGTCTTC
CAT-1	TAAGACTGACCAGGGCA	CAAACCTTGGTGAGATCGAA
E-CAD	GATCAAGTCAAGCGTGAGTCG	AGCCTCT CAATGGCGAACAC
HIF-1α	TGATTGCATCTCCATCTCCTAC	GACTCAAAGCGACAGATAACACG
KEAP1	CAACTTCGCTGAGCAGATTGGC	TGATGAGGGTCACCAGTTGGCA
NF-KB	GCAGCACTACTTCTTGACCACC	TCTGCTCCTGAGCATTGACGTC
NRF-2	CACATCCAGTCAGAAACCAGTGG	GGAATGTCTGCGCCAAAAGCTG
SLUG	CATGCCTGTCATACCACAAC	GGTGTCAGATGGAGGAGG
SNAIL	GCGAGCTGCAGGACTCTAAT	CCCGCAATGGTCCACAAAAC
SOD-1	AACTGCAACAGCTGTGGG	ACATTGCCCAGGTCTCCC
ZEB-1	GGCATACACCTACTCAACTACGG	TGGGCGGTGTAGAATCAGAGTC

Primer sequences (forward and reverse) used to amplify the genes, listed in alphabetical order.

Metabolite extraction from cell culture for LC-MS

At the end of treatment, cells were washed with a 0.9% NaCl solution (Sigma-Aldrich) and subsequently quenched with an ice-cold mixture of 70:30 acetonitrile:water (both from Honeywell, Wabash, IN, USA). The plates were then placed at −80°C for 10 min, followed by collection through scraping and sonication (twice for 5 s each, at 70% power). After centrifugation at 12,000×*g* for 10 min, the supernatant aqueous phases were collected in a glass insert and dried using a centrifugal vacuum concentrator (Concentrator plus/Vacufuge plus, Eppendorf, Hamburg, Germany) at 30°C for approximately 2.5 h. Finally, the samples were resuspended in 150 µL of H_2O before analysis.

LC-MS metabolic profiling

LC separation was conducted using an Agilent 1290 Infinity UHPLC system with an InfinityLab Poroshell 120 PFP column (2.1 × 100 mm, 2.7 µm; Agilent Technologies, Santa Clara, CA, USA). The mobile phase A consisted of water with 0.1% formic acid (both from Honeywell), while mobile phase B comprised acetonitrile with 0.1% formic acid. The injection volume was 10 µL, and the LC gradient conditions were as follows: 0 min: 100% A; 2 min: 100% A; 4 min: 99% A; 10 min: 98% A; 11 min: 70% A; 15 min: 70% A; and 16 min: 100% A with a 2-min post-run period. The flow rate was 0.2 mL/min, and the column temperature was maintained at 35°C. MS detection was performed using an Agilent 6550 iFunnel Q-TOF mass spectrometer equipped with a Dual JetStream source, operating in negative ionization mode. The specific MS parameters were as follows: gas temperature: 285°C; gas flow: 14 L/min; nebulizer pressure: 45 psig; sheath gas temperature: 330°C; sheath gas flow: 12 L/min; VCap: 3700 V; Fragmentor: 175 V; Skimmer: 65 V; and Octopole RF: 750 V. Active reference mass correction was achieved through a second nebulizer using masses with m/z values of 112.9855 and 1,033.9881. Data acquisition spanned the range of m/z 60–1,050. Subsequent data analysis and isotopic natural abundance correction were carried out using Agilent's MassHunter ProFinder software, as described in Bonanomi et al.[63]

Metabolomics statistical data analysis

Metabolomics data were analyzed using Metaboanalyst 5.0 (https://www.metaboanalyst.ca/). The raw data underwent logarithmic transformation (log10 scale) and normalization using Pareto scaling. Subsequently, statistical analysis was conducted by applying an unpaired t test or one-way ANOVA analysis with a significance threshold (*p* value) set at 0.05. To account for multiple testing, Benjamini and Hochberg false discovery rate correction was applied during *p* value computation. Data visualization of significant entities was achieved using a hierarchical clustering algorithm, allowing for the visualization of normalized intensity values and the clustering of both entities and conditions with similar metabolic fingerprints. Principal component analysis results were visualized through 2D score plots based on the first two components. Enrichment analysis on significant entities was performed using over representation analysis against a metabolite set library from SMPDB, involving 99 metabolite sets, to identify over-represented metabolite sets based on the hypergeometric test.

Cell cycle

Cell-cycle analysis was performed on 1×10^6 dissociated GBMs fixed in 70% ice-cold ethanol dropwise manner dispensed while mixing gently on a vortex and incubated on ice for 1 h. The cells were incubated with 50 µg/mL propidium iodide (Sigma-Aldrich), 3.8 mmol/L sodium citrate (Sigma-Aldrich), and 10 µg/mL RNase (Sigma-Aldrich) for 1 h in the dark and at room temperature. Samples were acquired through a FACS Calibur flow cytometer (BD

Biosciences, Franklin, NJ, USA). All data were analyzed using FlowJo software (Tree Star, Ashland, OR, USA).

Immunoblotting

Protein extracts (50 μg) of T98 and U251 scramble cell lines, treated with TMZ, treated with the miRNA675-5p inhibitor and treated with the inhibitor followed by TMZ treatment were loaded in triplicate and resolved on 7%–12% gradient polyacrylamide gels. The blots were incubated with rabbit polyclonal anti-RPTOR antibodies (Invitrogen, #42-4000; 1:1,000) and mouse monoclonal anti-β-actin antibodies (Sigma, A1978; 1:3,000). After washing, the membranes were incubated with secondary anti-rabbit antibody (Jackson ImmunoResearch Laboratories, West Grove, PA, USA; 111-035-003; 1:10,000) or anti-mouse (Jackson ImmunoResearch Laboratories, 115-035-003; 1:5,000) conjugated with horseradish peroxidase. The signals were visualized by chemiluminescence using the ECL Prime detection kit and the Image Quant LAS 4000 analysis system (GE Healthcare, Chicago, IL, USA). Band quantification was performed with Image Quant TL software (GE Healthcare), followed by statistical analysis (ANOVA + Tukey; $n = 3$; $p < 0.05$). RPTOR band intensities were normalized with respect to β-actin protein levels.

Statistical analysis

The *in vitro* experiments were repeated three times and led to reproducible results. The data are presented as the mean values ± SD of three independent experiments and were statistically analyzed using a t test or one- or two-way ANOVA, followed by Dunnett's or Bonferroni's multiple comparison and Prism 4 software (GraphPad Software Inc., San Diego, CA, USA).

DATA AVAILABILITY

The data supporting the results of this study can be obtained from the corresponding author upon reasonable request.

ACKNOWLEDGMENTS

This research was funded by PRIN 2022 TNPEM2022 (CUP G53D23004850006) and PRIN PNRR 2022 (CUP B53D23025920001).

The authors are also grateful to Luisa Aquino, Lorena Bonaldi, Clara Castoldi, and Gabriele Di Blasi for their advice and administrative support. The authors wish to thank Dr. Reem Mahmoud Fawzi Mahmoud Mohamed and Dr. Tamara Alonso Avila for their advice and skillful support for English revision.

AUTHOR CONTRIBUTIONS

C.M.: data curation, formal analysis, writing—original draft. M.B.: data curation, formal analysis, writing—original draft. A.G.: data curation, formal analysis. S.R.: data curation, formal analysis. C.P. and M.N.: data curation, formal analysis. D.G.: formal analysis, writing—review and editing. D.C.: data curation, formal analysis. D.P.: supervision. L. O.: conceptualization, formal analysis, supervision, writing—review and editing. A.L. D.: conceptualization, formal analysis, funding acquisition, supervision, writing—original draft, writing—review and editing.

DECLARATION OF INTERESTS

The authors declare no competing interests.

SUPPLEMENTAL INFORMATION

Supplemental information can be found online at https://doi.org/10.1016/j.omtn.2025.102647.

REFERENCES

1. Stupp, R., Hegi, M.E., Mason, W.P., van den Bent, M.J., Taphoorn, M.J.B., Janzer, R. C., Ludwin, S.K., Allgeier, A., Fisher, B., Belanger, K., et al. (2009). Effects of radiotherapy with concomitant and adjuvant temozolomide versus radiotherapy alone on survival in glioblastoma in a randomised phase III study: 5-year analysis of the EORTC-NCIC trial. Lancet Oncol. *10*, 459–466. https://doi.org/10.1016/S1470-2045(09)70025-7.
2. DeAngelis, L.M., and Wen, P.Y. (2018). Primary and Metastatic Tumors of the Nervous System. In Harrison's Principles of Internal Medicine, 20th ed., Shanahan. and Davis., eds. (McGraw-Hill Professional Publishing), p. p31. Chapter 86.
3. Louis, D.N., Perry, A., Reifenberger, G., Von Deimling, A., Figarella-Branger, D., Cavenee, W.K., Ohgaki, H., Wiestler, O.D., Kleihues, P., and Ellison, D.W. (2016). The 2016 World Health Organization Classification of Tumors of the Central Nervous System: A summary. Acta Neuropathol. *131*, 803–820. https://doi.org/10.1007/s00401-016-1545-1.
4. Pegg, A.E., and Byers, T.L. (1992). Repair of DNA containing O6-alkylguanine. FASEB J. *6*, 2302–2310. https://doi.org/10.1096/fasebj.6.6.1544541.
5. Huang, R., Chen, H., Liang, J., Li, Y., Yang, J., Luo, C., Tang, Y., Ding, Y., Liu, X., Yuan, Q., et al. (2021). Dual Role of Reactive Oxygen Species and their Application in Cancer Therapy. J. Cancer *12*, 5543–5561. https://doi.org/10.7150/jca.54699.
6. Weinberg, F., Ramnath, N., and Nagrath, D. (2019). Reactive Oxygen Species in the Tumor Microenvironment: An Overview. *Cancers* (Basel) *11*, 1191. https://doi.org/10.3390/cancers11081191.
7. Pudełek, M., Król, K., Catapano, J., Wróbel, T., Czyż, J., and Ryszawy, D. (2020). Epidermal Growth Factor (EGF) Augments the Invasive Potential of Human Glioblastoma Multiforme Cells via the Activation of Collaborative EGFR/ROS-Dependent Signaling. Int. J. Mol. Sci. *21*, 3605. https://doi.org/10.3390/ijms21103605.
8. Jin, L., Kiang, K.M.Y., Cheng, S.Y., and Leung, G.K.K. (2022). Pharmacological inhibition of serine synthesis enhances temozolomide efficacy by decreasing O^6-methylguanine DNA methyltransferase (MGMT) expression and reactive oxygen species (ROS)-mediated DNA damage in glioblastoma. Lab. Invest. *102*, 194–203. https://doi.org/10.1038/s41374-021-00666-7.
9. Sawai, S., Wong, P.F., and Ramasamy, T.S. (2022). Hypoxia-regulated microRNAs: the molecular drivers of tumor progression. Crit. Rev. Biochem. Mol. Biol. *57*, 351–376. https://doi.org/10.1080/10409238.2022.2088684.
10. Kaur, B., Khwaja, F.W., Severson, E.A., Matheny, S.L., Brat, D.J., and Van Meir, E.G. (2005). Hypoxia and the hypoxia-inducible-factor pathway in glioma growth and angiogenesis. Neuro Oncol. *7*, 134–153. https://doi.org/10.1215/S1152851704001115.
11. Moszyńska, A., Jaśkiewicz, M., Serocki, M., Cabaj, A., Crossman, D.K., Bartoszewska, S., Gebert, M., Dąbrowski, M., Collawn, J.F., and Bartoszewski, R. (2022). The hypoxia-induced changes in miRNA-mRNA in RNA-induced silencing complexes and HIF-2 induced miRNAs in human endothelial cells. FASEB J. *36*, e22412. https://doi.org/10.1096/fj.202101987R.
12. Shen, G., Li, X., Jia, Y.F., Piazza, G.A., and Xi, Y. (2013). Hypoxia-regulated microRNAs in human cancer. Acta Pharmacol. Sin. *34*, 336–341. https://doi.org/10.1038/aps.2012.195.
13. Costa, V., Lo Dico, A., Rizzo, A., Rajata, F., Tripodi, M., Alessandro, R., and Conigliaro, A. (2017). MiR-675-5p supports hypoxia induced epithelial to mesenchymal transition in colon cancer cells. Oncotarget *8*, 24292–24302. https://doi.org/10.18632/oncotarget.14464.
14. Lo Dico, A., Costa, V., Martelli, C., Diceglie, C., Rajata, F., Rizzo, A., Mancone, C., Tripodi, M., Ottobrini, L., Alessandro, R., and Conigliaro, A. (2016). MiR675-5p Acts on HIF-1α to Sustain Hypoxic Responses: A New Therapeutic Strategy for Glioma. Theranostics *6*, 1105–1118. https://doi.org/10.7150/thno.14700.
15. Saieva, L., Barreca, M.M., Zichittella, C., Prado, M.G., Tripodi, M., Alessandro, R., and Conigliaro, A. (2020). Hypoxia-Induced miR-675-5p Supports β-Catenin

Nuclear Localization by Regulating GSK3-β Activity in Colorectal Cancer Cell Lines. Int. J. Mol. Sci. *21*, 3832. https://doi.org/10.3390/ijms21113832.

16. Qutub, A.A., and Popel, A.S. (2008). Reactive oxygen species regulate hypoxia-inducible factor 1alpha differentially in cancer and ischemia. Mol. Cell Biol. *28*, 5106–5119. https://doi.org/10.1128/MCB.00060-08.

17. Nazarewicz, R.R., Dikalova, A., Bikineyeva, A., Ivanov, S., Kirilyuk, I.A., Grigor'ev, I. A., and Dikalov, S.I. (2013). Does scavenging of mitochondrial superoxide attenuate cancer prosurvival signaling pathways? Antioxid. Redox Signal. *19*, 344–349. https://doi.org/10.1089/ars.2013.5185.

18. Lo Dico, A., Martelli, C., Diceglie, C., Lucignani, G., and Ottobrini, L. (2018). Hypoxia-Inducible Factor-1α Activity as a Switch for Glioblastoma Responsiveness to Temozolomide. Front. Oncol. *8*, 249. https://doi.org/10.3389/fonc.2018.00249.

19. Lo Dico, A., Salvatore, D., Martelli, C., Ronchi, D., Diceglie, C., Lucignani, G., and Ottobrini, L. (2019). Intracellular Redox-Balance Involvement in Temozolomide Resistance-Related Molecular Mechanisms in Glioblastoma. Cells *8*, 1315. https://doi.org/10.3390/cells8111315.

20. Valtorta, S., Lo Dico, A., Raccagni, I., Gaglio, D., Belloli, S., Politi, L.S., Martelli, C., Diceglie, C., Bonanomi, M., Ercoli, G., et al. (2017). Metformin and temozolomide, a synergic option to overcome resistance in glioblastoma multiforme models. Oncotarget *8*, 113090–113104. https://doi.org/10.18632/oncotarget.23028.

21. Lo Dico, A., Valtorta, S., Ottobrini, L., and Moresco, R.M. (2019). Role of Metformin and AKT Axis Modulation in the Reversion of Hypoxia Induced TMZ-Resistance in Glioma Cells. Front. Oncol. *9*, 463. https://doi.org/10.3389/fonc.2019.00463.

22. Djamel-Eddine, Y.C., De Witte, O., Mélot, C., and Lefranc, F. (2019). Recurrent glioblastomas: Should we operate a second and even a third time? Interdiscip Neurosurg *18*, 100551. https://doi.org/10.1016/j.inat.2019.100551.

23. Tang, W., Wang, X., Chen, Y., Zhang, J., Chen, Y., and Lin, Z. (2015). CXCL12 and CXCR4 as predictive biomarkers of glioma recurrence pattern after total resection. Pathol. Biol. *63*, 190–198. https://doi.org/10.1016/j.patbio.2015.07.002.

24. Neville, I.S., Dos Santos, A.G., Almeida, C.C., Abaurre, L.B., Wayhs, S.Y., Feher, O., Teixeira, M.J., and Lepski, G. (2021). Reoperation for recurrent glioblastomas: What to expect? Surg. Neurol. Int. *12*, 42. https://doi.org/10.25259/SNI_538_2020.

25. Kouri, F.M., Jensen, S.A., and Stegh, A.H. (2012). The role of Bcl-2 family proteins in therapy responses of malignant astrocytic gliomas: Bcl2L12 and beyond. Sci. World J. *2012*, 838916. https://doi.org/10.1100/2012/838916.

26. Liu, H., and Tang, T. (2023). MAPK signaling pathway-based glioma subtypes, machine-learning risk model, and key hub proteins identification. Sci. Rep. *13*, 19055. https://doi.org/10.1038/s41598-023-45774-0.

27. Chao, M., Liu, N., Sun, Z., Jiang, Y., Jiang, T., Xv, M., Jia, L., Tu, Y., and Wang, L. (2020). TGF-β Signaling Promotes Glioma Progression Through Stabilizing Sox9. Front. Immunol. *11*, 592080. https://doi.org/10.3389/fimmu.2020.592080.

28. Ning, W., Qiu, Z., Ji, X., Wang, X., An, Y., Wang, S., and Zhang, H. (2020). The Prognostic Value of EMT in Glioma and its Role in the Glioma Immune Microenvironment. J. Mol. Neurosci. *70*, 1501–1511. https://doi.org/10.1007/s12031-020-01583-y.

29. Li, Y., Zhang, X., Wang, Z., Li, B., and Zhu, H. (2023). Modulation of redox homeostasis: A strategy to overcome cancer drug resistance. Front. Pharmacol. *14*, 1156538. https://doi.org/10.3389/fphar.2023.1156538.

30. Wang, Y., Qi, H., Liu, Y., Duan, C., Liu, X., Xia, T., Chen, D., Piao, H.l., and Liu, H.X. (2021). The double-edged roles of ROS in cancer prevention and therapy. Theranostics *11*, 4839–4857. https://doi.org/10.7150/thno.56747.

31. Zhou, S., Ye, W., Shao, Q., Zhang, M., and Liang, J. (2013). Nrf2 is a potential therapeutic target in radioresistance in human cancer. Crit. Rev. Oncol. Hematol. *88*, 706–715. https://doi.org/10.1016/j.critrevonc.2013.09.001.

32. Gruosso, T., Mieulet, V., Cardon, M., Bourachot, B., Kieffer, Y., Devun, F., Dubois, T., Dutreix, M., Vincent-Salomon, A., Miller, K.M., and Mechta-Grigoriou, F. (2016). Chronic oxidative stress promotes H2AX protein degradation and enhances chemosensitivity in breast cancer patients. EMBO Mol. Med. *8*, 527–549. https://doi.org/10.15252/emmm.201505891.

33. Jung, B.J., Yoo, H.S., Shin, S., Park, Y.J., and Jeon, S.M. (2018). Dysregulation of NRF2 in Cancer: from Molecular Mechanisms to Therapeutic Opportunities. Biomol. Ther. *26*, 57–68. https://doi.org/10.4062/biomolther.2017.195.

34. Godoy, P.R.D.V., Pour Khavari, A., Rizzo, M., Sakamoto-Hojo, E.T., and Haghdoost, S. (2020). Targeting NRF2, Regulator of Antioxidant System, to Sensitize Glioblastoma Neurosphere Cells to Radiation-Induced Oxidative Stress. Oxid. Med. Cell. Longev. *2020*, 2534643. https://doi.org/10.1155/2020/2534643.

35. Krajka-Kuźniak, V., and Baer-Dubowska, W. (2021). Modulation of Nrf2 and NF-κB Signaling Pathways by Naturally Occurring Compounds in Relation to Cancer Prevention and Therapy. Are Combinations Better Than Single Compounds? Int. J. Mol. Sci. *22*, 8223. https://doi.org/10.3390/ijms22158223.

36. Hamada, S., Matsumoto, R., and Masamune, A. (2022). HIF-1 and NRF2; Key Molecules for Malignant Phenotypes of Pancreatic Cancer. *Cancers* (Basel) *14*, 411. https://doi.org/10.3390/cancers14020411.

37. Bae, T., Hallis, S.P., and Kwak, M.K. (2024). Hypoxia, oxidative stress, and the interplay of HIFs and NRF2 signaling in cancer. Exp. Mol. Med. *56*, 501–514. https://doi.org/10.1038/s12276-024-01180-8.

38. Tang, T., Jia, Y., Liang, H., Han, Y., Cong, Z., Wang, H., and Ji, X. (2022). Knockdown of Nrf2 radiosensitizes glioma cells by inducing redox stress and apoptosis in hypoxia. Transl. Cancer Res. *11*, 4105–4116. https://doi.org/10.21037/tcr-22-1420.

39. de Souza, I., Monteiro, L.K.S., Guedes, C.B., Silva, M.M., Andrade-Tomaz, M., Contieri, B., Latancia, M.T., Mendes, D., Porchia, B.F.M.M., Lazarini, M., et al. (2022). High levels of *NRF2* sensitize temozolomide-resistant glioblastoma cells to ferroptosis via ABCC1/MRP1 upregulation. Cell Death Dis. *13*, 591. https://doi.org/10.1038/s41419-022-05044-9.

40. Grech, N., Dalli, T., Mizzi, S., Meilak, L., Calleja, N., and Zrinzo, A. (2020). Rising Incidence of Glioblastoma Multiforme in a Well-Defined Population. Cureus *12*, e8195. https://doi.org/10.7759/cureus.8195.

41. Saad, N.Y., Al-Kharsan, M., Garwick-Coppens, S.E., Chermahini, G.A., Harper, M. A., Palo, A., Boudreau, R.L., and Harper, S.Q. (2021). Human miRNA *miR-675* inhibits *DUX4* expression and may be exploited as a potential treatment for Facioscapulohumeral muscular dystrophy. Nat. Commun. *12*, 7128. https://doi.org/10.1038/s41467-021-27430-1.

42. Luo, H., Wang, J., Liu, D., Zang, S., Ma, N., Zhao, L., Zhang, L., Zhang, X., and Qiao, C. (2019). The lncRNA H19/miR-675 axis regulates myocardial ischemic and reperfusion injury by targeting PPARα. Mol. Immunol. *105*, 46–54. https://doi.org/10.1016/j.molimm.2018.11.011.

43. Li, X., Wang, H., Yao, B., Xu, W., Chen, J., and Zhou, X. (2016). lncRNA H19/miR-675 axis regulates cardiomyocyte apoptosis by targeting VDAC1 in diabetic cardiomyopathy. Sci. Rep. *6*, 36340. https://doi.org/10.1038/srep36340.

44. Trejo-Solís, C., Escamilla-Ramírez, Á., Gómez-Manzo, S., Castillo-Rodriguez, R.A., Palomares-Alonso, F., Castillo-Pérez, C., Jiménez-Farfán, D., Sánchez-García, A., and Gallardo-Pérez, J.C. (2025). The pentose phosphate pathway (PPP) in the glioma metabolism: A potent enhancer of malignancy. Biochimie *232*, 117–126. https://doi.org/10.1016/j.biochi.2025.01.013.

45. Kucharzewska, P., Christianson, H.C., and Belting, M. (2015). Global profiling of metabolic adaptation to hypoxic stress in human glioblastoma cells. PLoS One *10*, e0116740. https://doi.org/10.1371/journal.pone.0116740.

46. Kim, S.J., Park, S.J., Park, J., Cho, H.J., Shim, J.K., Seon, J., Choi, R.J., Yoon, S.J., Moon, J.H., Kim, E.H., et al. (2022). Dual inhibition of CPT1A and G6PD suppresses glioblastoma tumorspheres. J. Neuro Oncol. *160*, 677–689. https://doi.org/10.1007/s11060-022-04189-z.

47. Engel, A.L., Lorenz, N.I., Klann, K., Münch, C., Depner, C., Steinbach, J.P., Ronellenfitsch, M.W., and Luger, A.L. (2020). Serine-dependent redox homeostasis regulates glioblastoma cell survival. Br. J. Cancer *122*, 1391–13911398. https://doi.org/10.1038/s41416-020-0794-x.

48. Paul, B.D., Sbodio, J.I., and Snyder, S.H. (2018). Cysteine Metabolism in Neuronal Redox Homeostasis. Trends Pharmacol. Sci. *39*, 513–524. https://doi.org/10.1016/j.tips.2018.02.007.

49. Ruiz-Rodado, V., Dowdy, T., Lita, A., Kramp, T., Zhang, M., Jung, J., Dios-Esponera, A., Zhang, L., Herold-Mende, C.C., Camphausen, K., et al. (2022). Cysteine is a limiting factor for glioma proliferation and survival. Mol. Oncol. *16*, 1777–1794. https://doi.org/10.1002/1878-0261.13148.

50. Kay, E.J., Zanivan, S., and Rufini, A. (2023). Proline metabolism shapes the tumor microenvironment: from collagen deposition to immune evasion. Curr. Opin. Biotechnol. *84*, 103011. https://doi.org/10.1016/j.copbio.2023.103011.

51. Jin, J., Byun, J.K., Choi, Y.K., and Park, K.G. (2023). Targeting glutamine metabolism as a therapeutic strategy for cancer. Exp. Mol. Med. *55*, 706–715. https://doi.org/10.1038/s12276-023-00971-9.

52. Yang, C., Ko, B., Hensley, C.T., Jiang, L., Wasti, A.T., Kim, J., Sudderth, J., Calvaruso, M.A., Lumata, L., Mitsche, M., et al. (2014). Glutamine Oxidation Maintains the TCA Cycle and Cell Survival during Impaired Mitochondrial Pyruvate Transport. Mol. Cell *56*, 414–424. https://doi.org/10.1016/j.molcel.2014.09.025.

53. Pacifico, F., Leonardi, A., and Crescenzi, E. (2023). Glutamine Metabolism in Cancer Stem Cells: A Complex Liaison in the Tumor Microenvironment. Int. J. Mol. Sci. *24*, 2337. https://doi.org/10.3390/ijms24032337.

54. Beylerli, O., Sufianova, G., Shumadalova, A., Zhang, D., and Gareev, I. (2022). MicroRNAs-mediated regulation of glucose transporter (GLUT) expression in glioblastoma. Noncoding. RNA Res. *7*, 205–211. https://doi.org/10.1016/j.ncrna.2022.09.001.

55. Yang, C., Sudderth, J., Dang, T., Bachoo, R.M., McDonald, J.G., and DeBerardinis, R. J. (2009). Glioblastoma cells require glutamate dehydrogenase to survive impairments of glucose metabolism or Akt signaling. Cancer Res. *69*, 7986–7993. https://doi.org/10.1158/0008-5472.CAN-09-2266.

56. Tufail, M., Jiang, C.H., and Li, N. (2024). Altered metabolism in cancer: insights into energy pathways and therapeutic targets. Mol. Cancer *23*, 203. https://doi.org/10.1186/s12943-024-02119-3.

57. Schalm, S.S., and Blenis, J. (2002). Identification of a Conserved Motif Required for mTOR Signaling. Curr. Biol. *12*, 632–639. https://doi.org/10.1016/s0960-9822(02)00762-5.

58. Land, S.C., and Tee, A.R. (2007). Hypoxia-inducible factor 1alpha is regulated by the mammalian target of rapamycin (mTOR) via an mTOR signaling motif. J. Biol. Chem. *282*, 20534–20543. https://doi.org/10.1074/jbc.M611782200.

59. Wiecek, A.J., Cutty, S.J., Kornai, D., Parreno-Centeno, M., Gourmet, L.E., Tagliazucchi, G.M., Jacobson, D.H., Zhang, P., Xiong, L., Bond, G.L., et al. (2023). Genomic hallmarks and therapeutic implications of G0 cell cycle arrest in cancer. Genome Biol. *24*, 128. https://doi.org/10.1186/s13059-023-02963-4.

60. Min, M., and Spencer, S.L. (2019). Spontaneously slow-cycling subpopulations of human cells originate from activation of stress-response pathways. PLoS Biol. *17*, e3000178. https://doi.org/10.1371/journal.pbio.3000178.

61. Dazert, E., and Hall, M.N. (2011). mTOR signaling in disease. Curr. Opin. Cell Biol. *23*, 744–755. https://doi.org/10.1016/j.ceb.2011.09.003.

62. Livak, K.J., and Schmittgen, T.D. (2001). Analysis of relative gene expression data using real-time quantitative PCR and the 2(-Delta Delta C(T)) Method. Methods *25*, 402–408. https://doi.org/10.1006/meth.2001.1262.

63. Bonanomi, M., Salmistraro, N., Fiscon, G., Conte, F., Paci, P., Bravatà, V., Forte, G.I., Volpari, T., Scorza, M., Mastroianni, F., et al. (2021). Transcriptomics and Metabolomics Integration Reveals Redox-Dependent Metabolic Rewiring in Breast Cancer Cells. Cancers (Basel) *13*, 5058. https://doi.org/10.3390/cancers13205058.